ACS OMEGA

Article

Cite This: ACS Omega 2019, 4, 9952−9956

http://pubs.acs.org/journal/acsodf

Nanoindentation on Monolayer MoS_2 Kirigami

Beibei Wang,*[,†,‡] Aiichiro Nakano,[†,‡,§,∥] Priya D. Vashishta,[†,‡,§,∥] and Rajiv K. Kalia*[,†,‡,§,∥]

[†]Collaboratory of Advanced Computing and Simulations, [‡]Department of Physics and Astronomy, [§]Mork Family Department of Chemical Engineering and Materials Science, and [∥]Department of Computer Science, University of Southern California, Los Angeles, California 90089, United States

Supporting Information

ABSTRACT: Mechanical properties of materials can be altered significantly by the ancient art of kirigami. We study the mechanical properties of atomically thin kirigami membranes of MoS_2 using molecular dynamics simulations. Nanoindentation simulations are performed to study the mechanical response of rectangular and hexagonal kirigami structures. Dramatic changes are observed in the ductility of monolayer kirigami MoS_2 compared with those of a pristine MoS_2 monolayer. Load−displacement curves of kirigami structures exhibit negligible hysteresis, and kirigami structures display remarkable elastic recovery upon unloading. Defects formed at the edges and corners of kirigami structures play an important role in the mechanical response of the membranes.

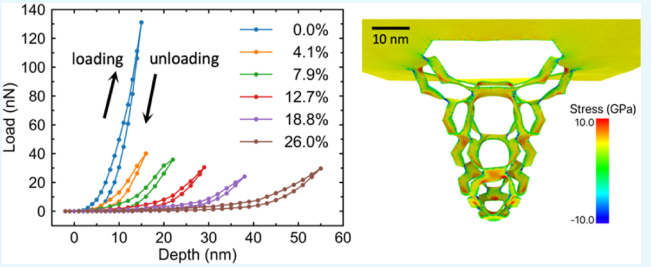

1. INTRODUCTION

Kirigami is an ancient art of paper cutting, two-dimensional (2D) layered materials such as graphene and transition-metal dichalcogenides, which are known to be as flexible as paper. Exploiting their flexibility, several research groups have recently applied kirigami to these 2D materials and made three-dimensional structures with exceptional mechanical and electrical properties.[1−6] For example, Blees et al. created graphene-based devices with two types of kirigami patterns: pyramid spiral spring and alternating offset cuts.[7] Their measurements of mechanical and electrical properties indicate the flexibility of kirigami graphene devices.

The flexibility of 2D materials is best characterized by the Föppl−von Kármán number[8,9] $\gamma = \frac{Y_{2D}L^2}{\kappa}$, where Y_{2D} represents the 2D Young's modulus of the material, κ is the out-of-plane bending stiffness, and L^2 is the area of the 2D material. Blees et al. have performed experimental analysis to obtain γ for graphene.[7] They find a large value of γ in the range of 10^5−10^7. We have estimated γ for a MoS_2 monolayer using the values of κ and the 2D Young's modulus ($Y_{2D} = Yh$, where h is the thickness of the sample and Y is Young's modulus) calculated from molecular dynamics (MD) simulation with the reactive empirical bond-order (REBO) force field.[10,11] The simulations by Xiong and Cao give κ to be around 10 eV and Y around 200 GPa.[12] With these values, the Föppl−von Kármán number for a 100 × 100 nm^2 sheet of MoS_2 is around 1.2 × 10^6, which is close to the value of γ for a standard sheet of paper. Such a large value of γ indicates that kirigami patterns can be created experimentally with a MoS_2 monolayer membrane.

We created two types of kirigami patterns in a monolayer of MoS_2 and examined the mechanical responses of those structures to nanoindentation by MD simulations. Nanoindentation is an important experimental technique to study the mechanical properties of materials at the nanoscale.[13−16] Bertolazzi et al. performed nanoindentation experiment to measure the mechanical strength of single and bilayer MoS_2.[17] They find that in-plane stiffness and breaking strength of ultrathin MoS_2 are comparable to those of stainless steel. Stewart and Spearot performed MD simulation to study nanoindentation on the basal plane of thin MoS_2.[1818] They investigated the incipient plastic deformation and found the local phase transformation using a slip vector analysis. Tan et al. have performed MD simulation to study the deflection dependence of monolayer graphene and obtain Young's modulus from indentation.[19]

Recently, a few experimental studies and MD simulations of 2D kirigami materials have also been reported. Shyu et al. reported a controlled kirigami patterning technique to engineer the elasticity of nanocomposite sheets.[20] They claim to have significantly improved the tensile capability of the stretchable conductor nanosheets and the electrical properties of the composites. Hanakata et al. have performed MD simulations to investigate the density and length of overlapping kirigami patterns in MoS_2 nanoribbon.[21] They find significant enhancement of tensile ductility and fracture strains of kirigami structures.

2. COMPUTATIONAL METHODS

Molecular dynamics (MD) simulations are performed to study the nanoindentation response of MoS_2 in the presence of kirigami patterns. We use reactive empirical bond-order

Received: March 20, 2019
Accepted: May 13, 2019
Published: June 7, 2019

DOI: 10.1021/acsomega.9b00771
ACS Omega 2019, 4, 9952−9956

(REBO) potential to model the interaction between Mo and S atoms in MoS_2.[10] The REBO potential accounts for changes in local atomic configurations of atoms. The binding energy of Mo−S system is expressed as

$$E_b = \frac{1}{2}\sum_{i\neq j} f_{ij}^c(r_{ij})\left[\left(1+\frac{Q}{r_{ij}}\right)A\, e^{-\alpha r_{ij}} - b_{ij}B\, e^{-\beta r_{ij}}\right] \quad (1)$$

where f_{ij}^c is a cutoff function, r_{ij} is the atomic distance between atoms i and j, b_{ij} is a bond-order function, and A, B, Q, α, and β are parameters for pairwise interactions.

In the work reported here, we use a conical diamond indenter (see Figure S1) in the MD simulations. To account for the size effect of the indenter, three indenter tips with diameters of 6, 9, and 12 nm are used in the simulations. The interaction between the indenter and MoS_2 kirigami structures is described by Lennard-Jones potentials between C, Mo, and S atoms.[22] However, to avoid the attraction between the indenter and MoS_2, we only keep the 12th-order repulsive term of the potential. The parameters including potential depth ϵ_{ij}, characteristic length σ_{ij}, and cutoff are listed in Table S1 in the Supporting Information.

We created hexagonal (H) and square (S) kirigami patterns of various sizes in a MoS_2 monolayer of size 100 × 100 nm^2 (see Figure S1). The patterns are created by removing specific Mo and S atoms in the monolayer MoS_2 nanosheets. The size of the MoS_2 nanosheet is chosen so that it is much larger than the indenter size. After equilibrating the system at 300 K for 5 million MD time steps (time step is 1 fs), the load is applied gradually. The indenter is pushed toward the center of the MoS_2 monolayer for 1 nm at the rate of 10 m/s. Subsequently, the system is relaxed for 0.2 million MD steps while the indenter is held fixed, and the average force is calculated during the holding phase. Periodic boundary conditions are applied parallel to the x−y plane, i.e., the basal plane of the MoS_2 structure. A 10 nm-wide peripheral region of MoS_2 is kept frozen to mimic a rigid platform. Along the z-direction, we use free boundary condition on both sides of MoS_2. The equations of motion for all atoms are integrated with the velocity-Verlet algorithm.

3. RESULTS AND DISCUSSION

Figure 1a displays the MD results for the load as a function of indenter displacement, i.e., indentation depth for kirigami structures with hexagonal (H) pattern of varying sizes. The patterns shown in panels Figure 1b−d cover, respectively, 4.1, 12.7, and 26.0% of the total area of the indented MoS_2 monolayer. The load−displacement curves, green, blue, and red corresponding to patterns in Figure 1b−d, indicate how the mechanical response changes with the area of kirigami patterns. Here, the maximum load is chosen to be just below the critical value at which the structure fractures. For the same applied load, the indentation depth increases almost linearly with the area of the kirigami pattern. The load-bearing capacity of kirigami structures increases significantly with the area of kirigami patterns. The maximum indentation depth for the smallest pattern (Figure 1b) is 15 nm and it increases to 30 and 55 nm for kirigami structures shown in Figure 1c,d. This indicates that these structures are much more flexible than the pristine MoS_2 monolayer. Furthermore, these structures exhibit very little hysteresis in the load−displacement curves and suffer less damage than the pristine MoS_2 monolayer.

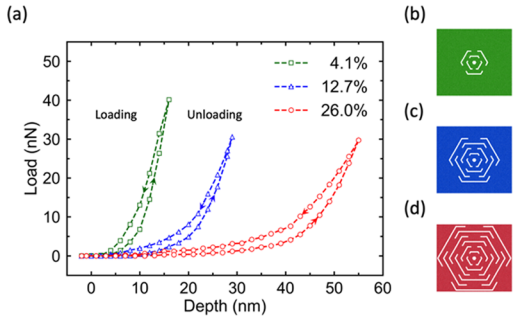

Figure 1. (a) Load−displacement curves for nanoindentation on MoS_2 with three kirigami structures of different area fractions. As a reference, the response of the MoS_2 monolayer without the kirigami structure is shown in Figure S2 in the Supporting Information. The green curve is the indentation response curve of the kirigami pattern shown in (b). The blue and red curves correspond to patterns shown in (c) and (d). The arrows in (a) pointing upward and downward indicate loading and unloading processes, respectively. The hysteresis in the load−displacement curves indicates irreversible damage in MoS_2 kirigami structures during nanoindentation. The MoS_2 kirigami pattern in (d) can be indented much more with a smaller load than the pristine MoS_2 monolayer.

Figure 1a shows that the hysteresis in the load−displacement curves remains nearly the same for structures (b) and (c). The hysteresis increases for the largest kirigami structure. This trend in hysteresis indicates that kirigami structures (b) and (c) have the same degree of plastic deformation, whereas the largest kirigami structure has undergone more plastic deformation and perhaps other kinds of defects have also formed in the system as a result of much larger indentation depth.

Evidently, increasing the area of kirigami pattern has a significant effect on the out-of-plane hardness of MoS_2. We have calculated the hardness of these kirigami structures from $H = \frac{P_{max}}{A}$, where P_{max} is the maximum applied load and A is the effective indented area. Knowing A and P_{max}, we find that the hardness decreases from 40.9 to 23.6 and 11.5 MPa as the kirigami area fraction increases from 4.1 to 12.7 and 26.0%. These values are much smaller than the hardness 519.6 MPa for a pristine MoS_2 monolayer.

We have calculated elastic modulii E_Y for these three structures from $E_Y = \frac{\sqrt{\pi}S}{2\beta\sqrt{A}}\frac{1}{}$, where S, the slope of the load−displacement curve at the maximum load upon unloading, also represents the stiffness of the MoS_2 kirigami structure. The values of S are 6.4, 3.7, and 1.8 N/m, respectively, for kirigami patterns (b)−(d). The quantity β accounts for the shape correction factor of the indenter, which is 1.0 for the conical indenter we use in the simulations. The elastic moduli for kirigami structures shown in panels (b)−(d) are 141.2, 81.6, and 39.7 MPa, respectively.

Figure 2a displays the MD results for the load as a function of indenter displacement in MoS_2 with square (S) kirigami patterns. The patterns shown in panels (b)−(d) cover, respectively, 5.4, 13.3, and 24.7% of the total area of the affected MoS_2 surface. Again, we observe that the out-of-plane flexibility of kirigami structures increases with the area of kirigami patterns. The maximum indentation depth before the failure of MoS_2 is 16 nm for the pattern shown in Figure 2c, while the indenter can go as deep as 38 nm for the pattern in Figure 2d before cracks develop at the corners of the pattern.

DOI: 10.1021/acsomega.9b00771
ACS Omega 2019, 4, 9952−9956

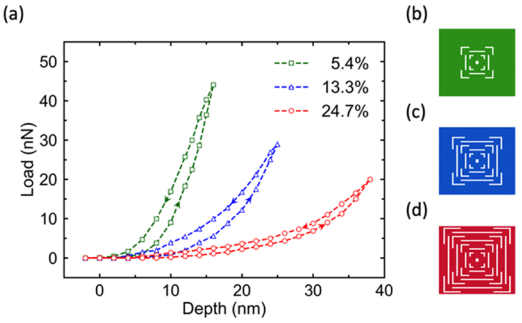

Figure 2. (a) Load−displacement curves for nanoindentation on square MoS_2 kirigami patterns shown in (b)−(d). The upward and downward arrows in each curve indicate loading and unloading processes, respectively. The areas of kirigami patterns in (b)−(d) are 5.4, 13.3, and 24.7%, respectively, of the total area of the MoS_2 monolayer. As in the case of hexagonal kirigami patterns, the hysteresis and hardness decrease significantly with an increase in the kirigami area.

The hardness of the three H kirigami patterns decreases from 42.6 to 10.5 MPa as the kirigami area increases from 5.4 to 24.7%. These values are again more than an order of magnitude smaller than that of a pristine MoS_2 monolayer but similar to the hardness of H patterns shown in Figure 1b−d.

The trend in Young's modulus for the three H structures confirms the similarity with S patterns. The hardness values are 7.3, 3.4, and 1.8 N/m, respectively, for kirigami patterns (b)−(d) in Figure 2. The elastic moduli for kirigami structures shown in panels (b)−(d) are 147.6, 68.8, and 36.3 MPa, respectively, very similar to Young's moduli of H kirigami structures shown in Figure 1.

We have investigated the effect of the indenter size on the mechanical response of the largest kirigami structures, where the area of the kirigami pattern is ∼25% of the total area of the MoS_2 monolayer. As shown in Figure 3, three conical indenters of diameters 60, 90, and 120 Å were used in the simulations. The load−displacement curves for hexagonal and square patterns are shown in Figure 3a,b, respectively. In the case of the H pattern, the effect of the indenter size is insignificant for indentation depths of 30 Å. Beyond that indentation depth, the force is larger for larger indenters in both the loading and unloading cycles. The hardness, elastic modulus, and stiffness for the three indenter sizes are listed in Table S2 in the Supporting Information. The load−displacement curves for the S kirigami structure are nearly the same for the three indenters, which implies that the indenter size has an insignificant effect on elastic properties, plastic deformation, and defect generation in S kirigami structures.

As each indenter is retracted, the force on the indenter due to MoS_2 deformation reduces to zero slowly. This indicates that the MoS_2 membrane is in contact with the indenter during unloading. The hysteresis indicates plastic deformation in kirigami structures even after the indenter is completely retracted. The indenter force at each indentation depth is more or less the same for different indenter sizes, which implies that the indenter size has an insignificant effect on the results. The elastic force arises mostly from the deformation of kirigami pattern outside the area of direct contact with the conical indenter.

The kirigami structures are extremely flexible and can withstand large strains and stresses without succumbing to fracture or failure. We have calculated stress distribution in kirigami membranes at various indentation depths. Figure 4 shows the stress distributions in hexagonal and square kirigami membranes indented with the same indenter of diameter 60 Å. The area fractions of these membranes are nearly the same (∼25%). Figure 4a,b shows the snapshots of hexagonal and square membranes under maximum loads. Above these loads, the ligaments of kirigami structures fracture and the membranes collapse. At the maximum applied loads, the indentation depth for the hexagonal (55 nm) structure is larger than that of the square (38 nm) kirigami structure. Stress distributions in the hexagonal and square kirigami structures at maximum applied loads are shown in Figure 4c,d. These are atomic-level stresses calculated from the virial expression for the stress tensor (see the Supporting Information). The stresses are compressive and large in the ligaments and corners of both kirigami patterns. The square pattern is evidently under larger compressive stress than the hexagonal kirigami structure. The stresses are negligible outside the kirigami patterns.

Beyond the elastic regime, compressive stresses tend to affect the corners and ligaments more than the rest of hexagonal and square kirigami patterns. Figure 5a shows the atomic configurations at a corner of a hexagonal kirigami structure before (left panel) and after (middle panel) indentation. Figure 5b presents the close-up views of a corner in the square kirigami structure before (left panel) and after (middle panel) indentation. As the applied load is increased, stresses weaken Mo−S bonds in the corner regions. Close to the maximum applied load, large compressive stresses break Mo−S bonds in both hexagonal and square kirigami structures. Most of the broken bonds are at the corners and a few of them

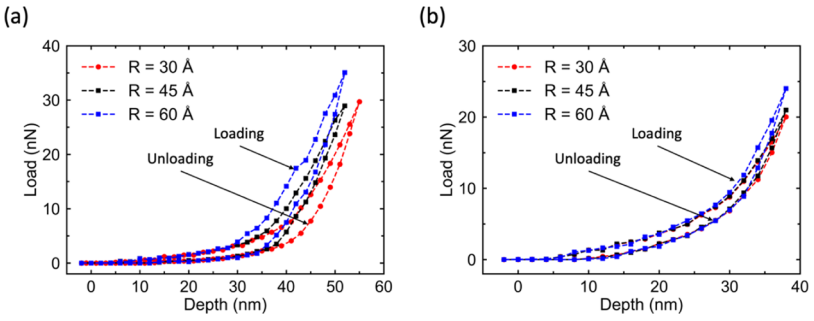

Figure 3. Effect of the indenter size on the two MoS_2 kirigami structures. (a) Load vs indentation depth for the hexagonal kirigami structure indented with indenters of radii 30, 45, and 60 Å. (b) Load vs indentation depth curves for the square kirigami structure indented with the same set of indenters. The area fractions of kirigami patterns in panels (a) and (b) are ∼25%.

DOI: 10.1021/acsomega.9b00771
ACS Omega 2019, 4, 9952−9956

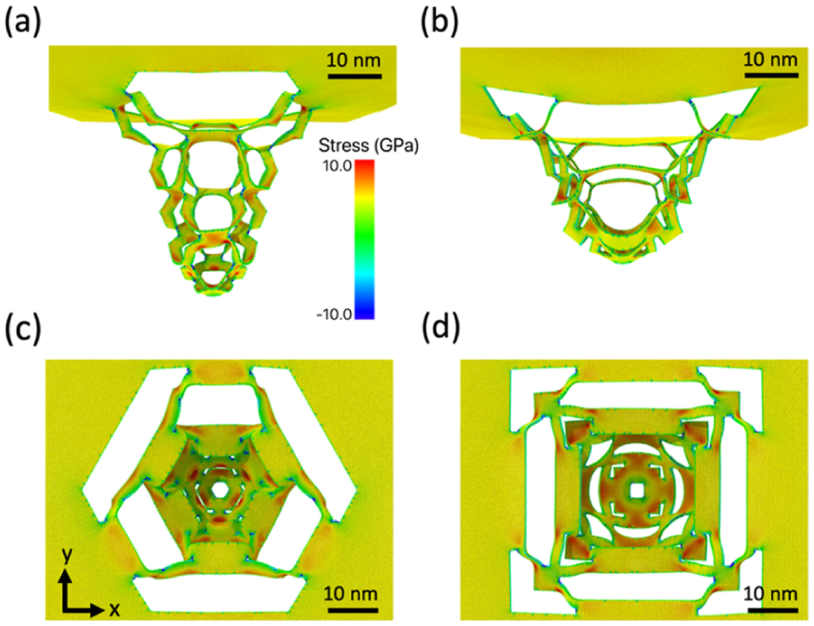

Figure 4. Stress distribution in the deformed MoS_2 membrane. (a) and (c) are side views of the deformed MoS_2 kirigami structures. MoS_2 layers form an elastic pyramid spring under nanoindentation (the indenter is removed from the view for better visualization of MoS_2). Stress is accumulated symmetrically around the corners and arms of kirigami patterns and goes up to 10 GPa. Panels (b) and (d) show the top views of deformed MoS_2 under nanoindentation. (Stress is calculated using per-atom volume and per-atom stress tensor averaged over 0.2 million MD steps).

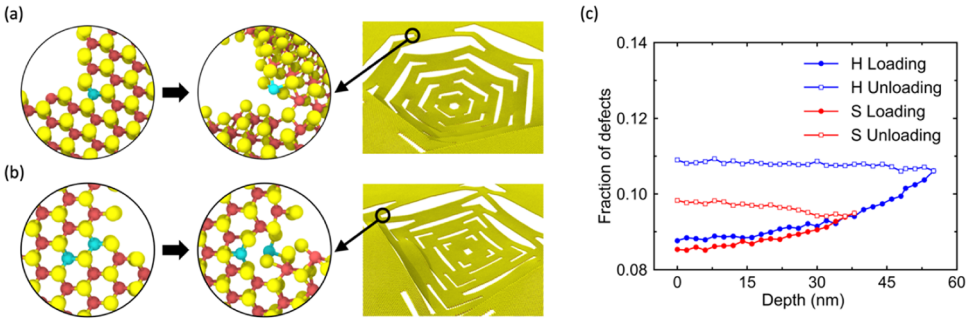

Figure 5. Evolution of defects induced by nanoindentation in MoS_2 kirigami structures. (a) Close-up views of a corner in a hexagonal kirigami pattern before indentation (left panel) and after indentation (middle panel). There are broken bonds and a nanocrack at the corner after the indenter is removed and the system is relaxed. (b) shows irreversible damage caused by indentation in a square kirigami structure. The left panel shows the atomic configuration at a corner of the square kirigami pattern before indentation. The middle panel is a close-up view of the same corner after indentation. Point defects shown in the middle panel persist even after the indenter has completely retracted and the kirigami structure has been relaxed for 2 million MD steps. The defect density in the two systems is shown in (c). Blue curves represent defect density in the hexagonal kirigami structure in Figure 1d during loading (lower curve) and unloading (flat upper curve) phases. Red curves in (c) show the defect density during loading and unloading in the square kirigami structure in Figure 2d.

in the ligaments of the kirigami patterns. These broken bonds give rise to point defects and nanoscale cracks. These defects do not heal upon unloading, and nanocracks also remain at the corners of kirigami patterns. We have estimated the density of defects by monitoring the number of broken bonds in the kirigami structures both during loading and unloading phases. These results are presented in Figure 5c. Blue curves show how the defect density increases upon loading in the hexagonal kirigami structure. The flat portion of the blue curve indicates that the defect density remains constant in the unloading phase. The lower red curve shows how the defect density increases with an increase in the applied load, and the upper red curve shows that the defect density remains constant during the entire unloading phase. Thus, the indentation leaves permanent damage in the kirigami structures.

4. CONCLUSIONS

In this simulation, we have created two kirigami patterns in the MoS_2 monolayer and investigated the nanoindentation response of these structures with different area fractions. We find that both hexagonal and square kirigami patterns can dramatically modulate the rigidity of a MoS_2 monolayer. A kirigami pattern with around 25% area of the MoS_2 membrane can reduce the out-of-plane stiffness by more than 10 times. The indenter size effect is insignificant since most of the deformation appears at ligaments and corners of the kirigami patterns and not where the indenter is directly in contact with the MoS_2 membrane. We have also identified two types of defects in the kirigami structure, which prevented complete recovery of the MoS_2 membrane from the nanoindentation and introduced hysteresis in the load−displacement curve for all of

DOI: 10.1021/acsomega.9b00771
ACS Omega 2019, 4, 9952−9956

the kirigami MoS_2 structures. We also propose nanoindentation experiment on this novel kirigami structures in the monolayer MoS_2 membrane.

■ ASSOCIATED CONTENT

Supporting Information

The Supporting Information is available free of charge on the ACS Publications website at DOI: 10.1021/acsomega.9b00771.

Schematic of nanoindentation simulation (Figure S1); the load−depth curves for all hexagonal MoS_2 kirigami structures (Figure S2); load−depth curve for all MoS_2 kirigami structures (Figure S3); load−depth curve for the pattern in Figure 1d in this paper (Figure S4); fraction of defects as a function of load (Figure S5); penetration of MoS_2 under indentation (Figure S6); parameters for L-J interactions between MoS_2 and the indenters (Table S1); mechanical properties for H patterns (Table S2); and mechanical properties for S patterns (Table S3) (PDF)

■ AUTHOR INFORMATION

Corresponding Authors

*E-mail: beibeiw@usc.edu (B.W.).
*E-mail: rkalia@usc.edu (R.K.K.).

ORCID

Beibei Wang: 0000-0002-9581-2698
Aiichiro Nakano: 0000-0003-3228-3896
Priya D. Vashishta: 0000-0003-4683-429X

Notes

The authors declare no competing financial interest.

■ ACKNOWLEDGMENTS

This work was supported by the U.S. Department of Energy, Office of Science, Basic Energy Sciences, Materials Science and Engineering Division, Grant DE-SC0018195. This work was performed, in part, at the Center for Integrated Nanotechnologies, an Office of Science User Facility operated for the U.S. Department of Energy (DOE) Office of Science. Sandia National Laboratories is a multimission laboratory managed and operated by the National Technology and Engineering Solutions of Sandia, LLC., a wholly owned subsidiary of Honeywell International, Inc., for the U.S. DOE's National Nuclear Security Administration under contract DE-NA-0003525. The views expressed in this article do not necessarily represent the views of the U.S. DOE or the United States Government.

■ REFERENCES

(1) Lee, W.; et al. Two-dimensional materials in functional three-dimensional architectures with applications in photodetection and imaging. *Nat. Commun.* **2018**, No. 1417.

(2) Jing, L.; et al. Kirigami metamaterials for reconfigurable toroidal circular dichroism. *NPG Asia Mater.* **2018**, *10*, 888−898.

(3) Xu, L.; Shyu, T. C.; Kotov, N. A. Origami and Kirigami Nanocomposites. *ACS Nano* **2017**, *11*, 7587−7599.

(4) Zhang, Y.; et al. A mechanically driven form of Kirigami as a route to 3D mesostructures in micro/nanomembranes. *Proc. Natl. Acad. Sci. U.S.A.* **2015**, *112*, 11757−11764.

(5) Guan, Y.-S.; Zhang, Z.; Tang, Y.; Yin, J.; Ren, S. Kirigami-Inspired Nanoconfined Polymer Conducting Nanosheets with 2000% Stretchability. *Adv. Mater.* **2018**, *30*, No. 1706390.

(6) Zheng, W.; et al. Kirigami-Inspired Highly Stretchable Nanoscale Devices Using Multidimensional Deformation of Monolayer MoS_2. *Chem. Mater.* **2018**, *30*, 6063−6070.

(7) Blees, M. K.; et al. Graphene kirigami. *Nature* **2015**, *524*, 204−207.

(8) Föppl, A. *Vorlesungen über technische Mechanik*; B.G. Teubner: Bd. 5. Leipzig, Germany, 1907; pp 132.

(9) von Kármán, T. Festigkeitsproblem im Maschinenbau. *Encyk. D. Math. Wiss. IV* **1910**, 311−385.

(10) Liang, T.; Phillpot, S. R.; Sinnott, S. B. Parametrization of a reactive many-body potential for Mo−S systems. *Phys. Rev. B* **2009**, *79*, No. 245110.

(11) Liang, T.; Phillpot, S. R.; Sinnott, S. B. Erratum: Parametrization of a reactive many-body potential for Mo - S systems. *Phys. Rev. B* **2012**, *85*, 2−3.

(12) Xiong, S.; Cao, G. Bending response of single layer MoS_2. *Nanotechnology* **2016**, *27*, No. 105701.

(13) Liu, K.; et al. Elastic properties of chemical-vapor-deposited monolayer MoS2, WS2, and their bilayer heterostructures. *Nano Lett.* **2014**, *14*, 5097−5103.

(14) Lee, C.; Wei, X.; Kysar, J. W.; Hone, J. Measurement of the Elastic Properties and Intrinsic Strength of Monolayer Graphene. *Science* **2008**, *321*, 385−388.

(15) Churnside, A. B.; et al. Routine and Timely Sub-picoNewton Force Stability and Precision for Biological Applications of Atomic Force Microscopy. *Nano Lett.* **2012**, *12*, 3557−3561.

(16) Huang, M.; Pascal, T. A.; Kim, H.; Goddard, W. A.; Greer, J. R. Electronic−Mechanical Coupling in Graphene from in situ Nanoindentation Experiments and Multiscale Atomistic Simulations. *Nano Lett.* **2011**, *11*, 1241−1246.

(17) Bertolazzi, S.; Brivio, J.; Kis, A. Stretching and Breaking of Ultrathin MoS 2. *ACS Nano* **2011**, *5*, 9703−9709.

(18) Stewart, J. A.; Spearot, D. E. Atomistic simulations of nanoindentation on the basal plane of crystalline molybdenum disulfide (MoS_2). *Modell. Simul. Mater. Sci. Eng.* **2013**, *21*, No. 045003.

(19) Tan, X.; et al. Nanoindentation models and Young's modulus of monolayer graphene: A molecular dynamics study. *Appl. Phys. Lett.* **2013**, *102*, No. 071908.

(20) Shyu, T. C.; et al. A kirigami approach to engineering elasticity in nanocomposites through patterned defects. *Nat. Mater.* **2015**, *14*, 785−789.

(21) Hanakata, P. Z.; Qi, Z.; Campbell, D. K.; Park, H. S. Highly stretchable MoS_2 kirigami. *Nanoscale* **2016**, *8*, 458−463.

(22) Liu, B.; et al. Thermal transport in a graphene-MoS_2 bilayer heterostructure: a molecular dynamics study. *RSC Adv.* **2015**, *5*, 29193−29200.

DOI: 10.1021/acsomega.9b00771
ACS Omega 2019, 4, 9952−9956